Multiple Ionic-Plasmon Resonances in Naturally Occurring Multiwall Nanotubes: Infrared Spectra of Chrysotile Asbestos

Etienne Balan,[1] Francesco Mauri,[1] Céline Lemaire,[1] Christian Brouder,[1] François Guyot,[1] A. Marco Saitta,[2] and Bertrand Devouard[3]

[1]*Laboratoire de Minéralogie Cristallographie, Case 115, 4 Place Jussieu, 75252 Paris Cedex 05, France*
[2]*Laboratoire de Physique des Milieux Condensés, 4 Place Jussieu, 75252 Paris Cedex 05, France*
[3]*Laboratoire Magmas et Volcans, 5 rue Kessler, 63038 Clermont-Ferrand Cedex, France*

(Received 21 May 2002; published 4 October 2002)

Chrysotile asbestos is formed by densely packed bundles of multiwall hollow nanotubes. Each wall in the nanotubes is a cylindrically wrapped layer of $Mg_3Si_2O_5(OH)_4$. We show by experiment and theory that the infrared spectra of chrysotile present multiple ionic-plasmon resonances in the Si-O stretching bands. These collective charge excitations are universal features of the nanotubes that are obtained by cylindrically wrapping an anisotropic material. The multiple plasmons can be observed if the width of the resonances is sufficiently small as in chrysotile.

DOI: 10.1103/PhysRevLett.89.177401 PACS numbers: 78.67.Ch, 63.22.+m, 73.20.Mf, 91.60.–x

The interaction of nanostructures with electromagnetic waves has recently received increasing attention, both because of fundamental and technological issues. The frequency dependence of this interaction is governed by different phenomena according to the characteristic size of the nanostructure template. The regime dominated by interference and diffraction occurs for particle sizes close to the wavelength of light as, e.g., in photonic crystals or in opals. The regime dominated by quantum mechanics occurs for sizes close to or smaller than a few nanometers such as in quantum dots or nanocrystals. Between these two regimes, a third regime occurs where the frequency dependence is dictated by collective charge excitations, i.e., by confined plasmons [1–6]. In this regime, an interesting phenomenon occurs in multiwall nanotubes that are obtained by wrapping around cylindrical layers of an anisotropic material, as in carbon [1,4,5] or WS_2 [6] nanotubes. In particular, the macroscopic dielectric tensor, $\vec{\vec{\epsilon}}(\omega)$, of the nanotubes can present *multiple* confined plasmon resonances that correspond to a *single* resonance in the dielectric tensor of the same material with flat planar layers. Such a phenomenon has been observed in theoretical calculations [5]. Experimental measurements exist in the energy range of electronic excitations ($\omega \simeq$ 5–25 eV) [2,4–6]. However, in these experiments, the multipeak spectrum is hidden by the large width of the electronic resonances of the corresponding planar materials [5].

In this Letter, we show that the resonances of $\vec{\vec{\epsilon}}(\omega)$ related to the ionic vibrations, in the infrared (IR) range ($\omega \simeq 0.1$ eV), are better candidates for the detection of multipeak spectra produced by collective charge excitations. In fact, the ionic resonances are much sharper than those related to the electronic excitations. Thus, in ionic materials with intense IR activity, multiple ionic plasmons could be expected. By experiment and theory, we prove that the IR spectra of chrysotile asbestos present, indeed, multiple ionic-plasmon peaks related to its peculiar tubular nanostucture.

Chrysotile asbestos is an example of natural multiwall hollow nanotubes with $Mg_3Si_2O_5(OH)_4$ composition, belonging to the group of serpentine minerals. These minerals are formed by stacking layers, each containing a pseudohexagonal silica sheet of corner-shared SiO_4 units linked to a sheet of edge sharing $MgO_2(OH)_4$ octahedra (Fig. 1). The OH groups located at the top of the octahedral sheet are H bonded with the O of the basal plane of the next layer. These minerals present cylindrically wrapped layers in chrysotile, corrugated layers in antigorite, and flat layers in lizardite [7,8]. The structural relation between chrysotile and lizardite is the same as that between C nanotubes and graphite. Chrysotile nanotubes present outer and inner diameters of 240–600 and 50–100 Å, respectively (Fig. 2). The tubes are arranged as densely packed bundles of parallel fibers.

We measure the IR spectra, in transmission and attenuated total reflectance (ATR), of a chrysotile sample. The

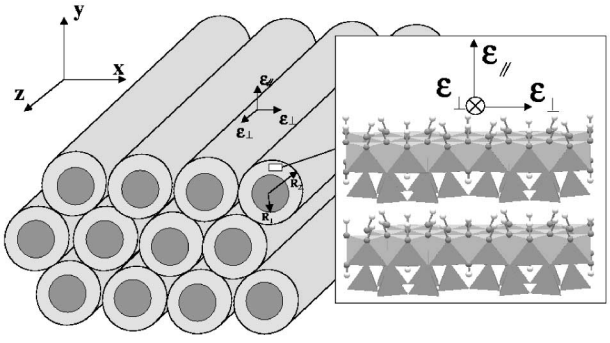

FIG. 1. Multiwall nanotubes of chrysotile, arranged as a hexagonal close-packed array. The cylinders are infinitely long in the z direction. Inset: Structure of lizardite showing the stacking of two layers.

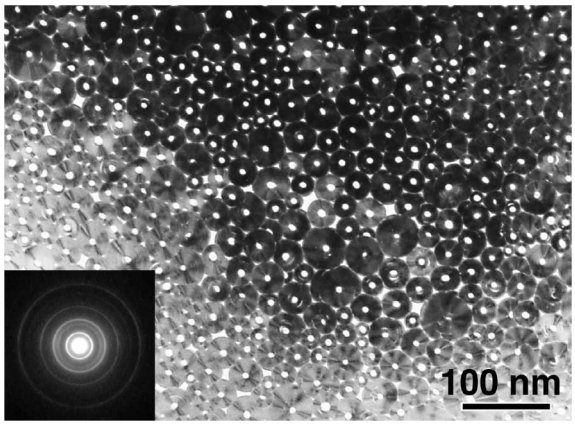

FIG. 2. Transmission electron micrography of the investigated chrysotile sample (Salt River Canyon, Arizona), viewed along the tube axes. Inset: Selected area electron diffraction pattern showing the parallel texture of chrysotile tubes.

sample, characterized by transmission electron microscopy and electron microprobe, consists of pure chrysotile (Fig. 2). The IR powder spectrum of chrysotile, compared to that of the flat-layered variety lizardite, displays a strong absorption band at 1018 cm^{-1} in the range of Si-O stretching vibrations (Fig. 3) (see also [9–12]). The shoulder observed at 1018 cm^{-1} in the lizardite spectrum is indeed related to chrysotile and polygonal serpentine contaminations present in a low amount in natural lizardite samples [11,13]. In the IR powder spectrum of lizardite, the band at 1084 cm^{-1} (L_1, Table I) is related to the out-of-plane (perpendicular to the layers) Si-O stretching mode, whereas that at 951 cm^{-1} (L_2, Table I) is related to the two degenerate in-plane (parallel to the layers) Si-O stretching modes [13]. The bands at 961 and 1018 cm^{-1} of chrysotile were previously related to the lift of this degeneracy by the bending of the tetrahedral sheets [10]. We better constrain the dependence of the IR spectrum as a function of the polarization of the incident wave, by recording the ATR IR spectra of an oriented chrysotile aggregate. In this experiment, the sample is pressed onto a Ge crystal. The spectrum of the IR light propagating in the Ge crystal and reflected at the chrysotile/Ge interface is recorded. The IR light has an incidence angle of 45°. The propagation and electric field vectors of the incident wave are set either parallel or perpendicular to the fiber axis and to the incidence plane, respectively (Fig. 4). The ATR spectrum recorded with the electric field vector parallel to the fiber axis displays only one band, whereas the three other spectra display three bands.

Since the size of the nanostructure template is much smaller than the wavelength of light, the IR spectrum is fully defined by the macroscopic dielectric tensor of chrysotile $\vec{\vec{\epsilon}}_C(\omega)$. To model the spectra, we consider, for simplicity, a nanostructured material composed of a close-packed array of monodispersed nanotubes (Fig. 1). An accurate effective medium theory has been derived for such systems [4]. However, here we compute $\vec{\vec{\epsilon}}_C(\omega)$ from the polarizability of a single tube using a simple Clausius-Mossotti model, given the approximations made on the size distribution and on the arrangement of the tubes.

The polarizability $\vec{\vec{\alpha}}(\omega)$ is calculated from the macroscopic dielectric tensor of the planar material, lizardite. The dielectric properties of an isolated tube in vacuum can be derived by assuming that the chrysotile tube is a dielectric continuum, locally identical to lizardite. Thus, the layer curvature is accounted for only at the macroscopic scale, as in Refs. [1,4,6]. The low-frequency

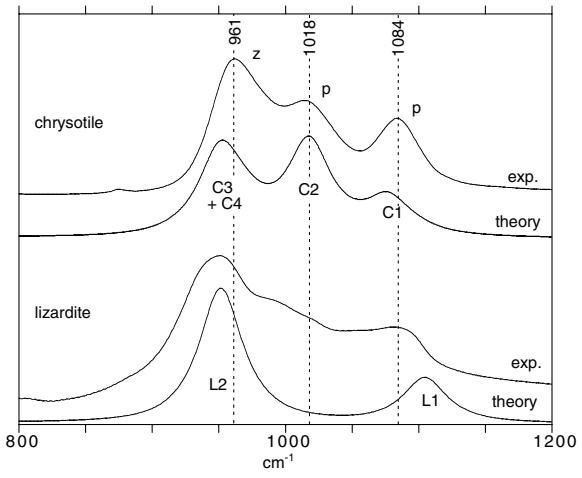

FIG. 3. Transmission powder IR absorption spectra of chrysotile and lizardite in KBr pellets (absorbance units). Spectra are recorded at room temperature using an FT-IR spectrometer Nicolet Magna 560 with a resolution of 2 cm^{-1}. z and p denote polarizations parallel and perpendicular to the tube axis, respectively.

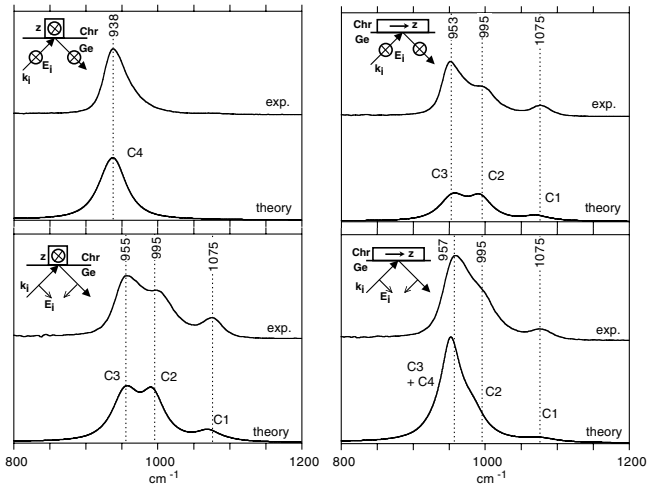

FIG. 4. Attenuated total reflectance IR spectra of chrysotile. Spectra in absorbance units are recorded with an ATR Thunderdome device equipped with an AgBr polarizer. The orientation of the chrysotile aggregate with respect to the incident IR wave is indicated; Chr: chrysotile; Ge: germanium crystal.

TABLE I. Theoretical transverse optical (TO) modes and corresponding resonances of the IR spectra. Experimental values in parentheses. With || and ⊥, we indicate the Si-O modes perpendicular and parallel to the $Mg_3Si_2O_5(OH)_4$ layers, and with $\mathbf{u}_r$, $\mathbf{u}_\varphi$, and $\mathbf{u}_z$, the dominant cylindrical polarization.

	Polarization	TO	Label	Transmission	ATR
Lizardite	||	1045	L_1	1105 (1084)	···
	⊥	951	L_2	951 (951)	···
Chrysotile	|| $\mathbf{u}_r$	1045	C_1	1077 (1084)	1071 (1075)
	⊥ $\mathbf{u}_\varphi$	951	C_2	1018 (1018)	991 (995)
	⊥ $\mathbf{u}_\varphi$	951	C_3	972	955 (955)
	⊥ $\mathbf{u}_z$	951	C_4	951 (961)	938 (938)

dielectric tensor of lizardite, $\overleftrightarrow{\epsilon}_L(\omega)$, can be written in Cartesian coordinates as

$$\overleftrightarrow{\epsilon}_L(\omega) = \epsilon_\perp(\omega)\mathbf{u}_x\mathbf{u}_x + \epsilon_{||}(\omega)\mathbf{u}_y\mathbf{u}_y + \epsilon_\perp(\omega)\mathbf{u}_z\mathbf{u}_z, \quad (1)$$

where $\mathbf{u}_y$ corresponds to the c axis of the lizardite hexagonal structure, and ω is the frequency of the IR wave. In Ref. [13], we have obtained the theoretical $\overleftrightarrow{\epsilon}_L(\omega)$ from the dynamical matrix and the effective charge tensors. These quantities were calculated from first principles using density functional perturbation theory [14]. In the present study, we use $\overleftrightarrow{\epsilon}_L(\omega)$ of Ref. [13] calculated with a damping coefficient of 16 cm^{-1}. However, to better fit the experimental IR spectrum of lizardite, we shift the transverse optical frequency of the two degenerate in-plane Si-O stretching modes from the theoretical value of 915 cm^{-1} [13] to the experimental value of 951 cm^{-1}. The resulting theoretical IR powder spectrum of lizardite, obtained following [13,15], is reported in Fig. 3.

The microscopic dielectric tensor of a chrysotile tube is

$$\overleftrightarrow{\epsilon}_{\mu C}(\varphi, r, \omega) = \epsilon_\perp(\omega)\mathbf{u}_z\mathbf{u}_z + \epsilon_{||}(\omega)\mathbf{u}_r\mathbf{u}_r + \epsilon_\perp(\omega)\mathbf{u}_\varphi\mathbf{u}_\varphi, \quad (2)$$

for $R_1 < r < R_2$, and $\overleftrightarrow{\epsilon}_{\mu C}(\varphi, r, \omega) = 1$ otherwise. Here $\mathbf{u}_z$, $\mathbf{u}_r$, and $\mathbf{u}_\varphi$ are now the unitary basis vectors of cylindrical coordinates and R_1 and R_2 are the inner and outer radii of the tube.

The polarizability of a single tube is obtained from the electric field induced by a quasistatic external field, $\mathbf{E}_{ext}$. The component of the electric field parallel to the cylindrical axis is homogeneous. The perpendicular component of the electric field is $\mathbf{E}(\varphi, r, \omega) = -\nabla V(\varphi, r, \omega)$. The electric field corresponding to a perpendicular external field $\mathbf{E}_{ext}$ is derived from the first Maxwell equation:

$$\nabla \cdot [\overleftrightarrow{\epsilon}_{\mu C}(\varphi, r, \omega) \cdot \mathbf{E}(\varphi, r, \omega)] = 0, \quad (3)$$

with the boundary condition $\mathbf{E}(\varphi, \infty, \omega) = \mathbf{E}_{ext}$. The electrostatic potential solution of Eq. (3) has the following form:

$$V(\varphi, r, \omega) = a_1 r \cos\varphi, \quad (4)$$

$$V(\varphi, r, \omega) = [a_2 r^{\Delta(\omega)} + b_2 r^{-\Delta(\omega)}]\cos\varphi, \quad (5)$$

$$V(\varphi, r, \omega) = (-E_{ext} r + b_3 r^{-1})\cos\varphi, \quad (6)$$

for $r < R_1$, $R_1 < r < R_2$, and $r > R_2$, respectively. Here, $\Delta(\omega) = \sqrt{\epsilon_\perp(\omega)/\epsilon_{||}(\omega)}$ and the scalar quantities a_1, a_2, b_2, and b_3 are determined by the continuity of $V(\varphi, r, \omega)$ and of the radial component of $\overleftrightarrow{\epsilon}_{\mu C}(\varphi, r, \omega) \cdot \mathbf{E}(\varphi, r, \omega)$ at the inner and outer surfaces of the tube. From these expressions, the transverse polarizability of the single tube $\alpha_p(\omega)$ can be derived [Eq. (4) of [1]]. The macroscopic dielectric tensor of chrysotile, $\overleftrightarrow{\epsilon}_C(\omega)$, is then obtained using an effective medium approach of Clausius-Mossotti type [4]:

$$\epsilon_{C,z}(\omega) = f'\epsilon_\perp(\omega) + (1 - f'), \quad (7)$$

$$\epsilon_{C,p}(\omega) = 1 + \frac{f\alpha_p(\omega)}{1 - f\alpha_p(\omega)/2}, \quad (8)$$

where $\epsilon_{C,z}(\omega)$ and $\epsilon_{C,p}(\omega)$ correspond to the components of $\overleftrightarrow{\epsilon}_C(\omega)$ parallel and perpendicular to the cylindrical axis, respectively, f is the volume fraction occupied by the tubes, $f \simeq 0.9$ for a close-packed arrangement of the tubes and $f' = f[1 - (R_1/R_2)^2]$. From these equations, it can be shown that a single resonance in the dielectric tensor of the flat planar material, $\overleftrightarrow{\epsilon}_L(\omega)$, can produce multiple resonances in $\alpha_p(\omega)$, and therefore in the macroscopic dielectric constant $\epsilon_{C,p}(\omega)$. This behavior has been observed in Ref. [5] for onionlike particles. The frequency for which confined plasmons occur can be obtained as the nonzero solutions of Eqs. (4)–(6), with $\mathbf{E}_{ext} = 0$. In the limit of a vanishing damping coefficient, these resonances occur when $D(\omega) = -i\Delta(\omega)$ is real and satisfies

$$D(\omega)\log(R_2/R_1) = -2\text{atan}[\epsilon_{||}(\omega)D(\omega)] + k\pi, \quad (9)$$

where k is an integer. This equation admits an infinity of solutions because of the divergence of $\overleftrightarrow{\epsilon}_L(\omega)$ at a resonance with zero damping. In practice, the finite width of the resonances of $\overleftrightarrow{\epsilon}_L(\omega)$ leads to a finite number of resonances of $\overleftrightarrow{\epsilon}_C(\omega)$, increasing with a decreasing ratio R_1/R_2.

To calculate the ATR spectra, we compute the reflection coefficient of an electromagnetic wave incident on a flat interface between the chrysotile medium, with dielectric tensor $\overleftrightarrow{\epsilon}_C(\omega)$, and a Ge medium, with isotropic dielectric tensor equal to 16. The theoretical spectrum in absorbance units is obtained as minus the logarithm of the reflection coefficient (Fig. 4). The major features and the changes of the spectra as a function of the polarization of the incident wave are very well reproduced by our calculations, with a ratio $R_1/R_2 = 0.1$, comparable with that observed by TEM (Fig. 2). The spectrum obtained with the electric field parallel to the fiber axis (Fig. 4, first panel) is described by $\epsilon_{C,z}(\omega)$ and displays a single band (C_4, Table I). The spectra obtained with the electric field perpendicular to the fiber axis (Fig. 4, second and third panels) are described by $\epsilon_{C,p}(\omega)$ and display three resonances (C_3, C_2, and C_1, Table I). Finally, the spectrum

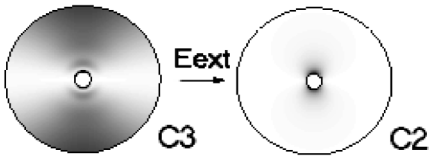

FIG. 5. Dissipated power density in an isolated nanotube at the resonances C_2 and C_3. The darker gray indicates larger dissipation. The arrow shows the direction of $\mathbf{E}_{\text{ext}}$.

obtained with the geometry of Fig. 4, last panel, contains resonances related to both $\epsilon_{C,p}(\omega)$ and $\epsilon_{C,z}(\omega)$.

The theoretical powder IR transmission spectrum of chrysotile is computed using $\vec{\epsilon}_C(\omega)$ as in Ref. [15]. In this case, we consider that micrometric chrysotile particles are elongated along the z axis and inserted in a homogeneous KBr medium. An excellent agreement between the theoretical and the experimental spectrum is obtained (Fig. 3). In particular, the calculation reproduces the presence and the position of the strong absorption band at 1018 cm^{-1}, characteristic of chrysotile. By an analysis of the theoretical spectra, we can correlate the peaks observed in ATR to those observed in transmission. In particular, we find that the peaks at 1084 and 1018 cm^{-1} in transmission are associated to the resonances C_1 and C_2, whereas the resonance at 961 cm^{-1} is mainly associated to C_4, and in a minor proportion to C_3. The frequency shifts and intensity changes of the bands between the ATR and the transmission spectra arise from the different geometry of the two experimental setups, and are reproduced by our calculations.

Our theoretical investigation of the IR spectrum of chrysotile also provides an unambiguous assignment of the resonances with respect to the vibrational modes of the layers, Table I. The out-of-plane Si-O stretching mode leads to C_1. The in-plane Si-O stretching mode polarized parallel to the cylindrical axis of the tube leads to C_4. The other in-plane Si-O stretching mode, perpendicular to the cylindrical axis, leads to the two resonances C_2 and C_3, that correspond to the solutions of Eq. (9) for $k = 1$ and $k = 2$, respectively. Therefore, the resonances C_2 and C_3 are related to two distinct localized ionic plasmons which originate from the same resonance in the dielectric tensor of lizardite. We study the spatial extension of these two plasmons by looking, in Fig. 5, at the spatial distribution of the dissipated power density, $W(\varphi, r, \omega) = \omega/(2\pi)\text{Im}[\mathbf{E}(\varphi, r, \omega)^* \cdot \vec{\epsilon}_{\mu C}(\varphi, r, \omega) \cdot \mathbf{E}(\varphi, r, \omega)]$ [15]. The resonance C_2 is related to a surface plasmon localized at the internal surface of the nanotube. The resonance C_3 is distributed over the whole tube, and presents two nodes close to the inner surface. Note that, in our calculations, the two in-plane Si-O stretching modes in the microscopic dielectric tensor $\vec{\epsilon}_{\mu C}(\varphi, r, \omega)$ are still degenerate. Therefore, the splitting of the Si-O stretching absorption bands in the IR spectra of chrysotile is not due to a distortion of the microscopic geometry of the tetrahedral sheets produced by the bending, as previously suggested [10], but to the macroscopic electric field induced by the ionic vibrational motion. This electric field is present for the in-plane Si-O stretching mode perpendicular to the tube axis but not for the other mode parallel to the tube axis.

In conclusion, we have shown, by experiment and theory, that multiple plasmons are observed in the IR spectra of chrysotile nanotubes. In particular, a *single* in-plane Si-O stretching mode of the $Mg_3Si_2O_5(OH)_4$ layer produces *two* resonances in the polarizability of chrysotile. We have predicted that the number of resonances increases with a decreasing width of the vibrational modes and/or a decreasing ratio between the inner and outer radii of the nanotubes. Thus, we anticipate that more resonances should be detected in chrysotile samples or other nanotube systems which optimize these parameters. Finally, the IR plasmon resonances could become a tool to monitor the geometrical parameters of nanotube based materials.

Calculations were performed at the IDRIS, and TEM work at the French INSU National Facility, CRMC2-CNRS, Marseille. This is IPGP contribution 1841.

[1] L. Henrard and P. Lambin, J. Phys. B **29**, 5127 (1996).
[2] W. A. de Heer, W. S. Bacsa, A. Châtelain, T. Gerfin, R. Humphrey-Baker, L. Forro, and D. Ugarte, Science **268**, 845 (1995).
[3] F. J. Garcia-Vidal and J. B. Pendry, Phys. Rev. Lett. **77**, 1163 (1996).
[4] F. J. Garcia-Vidal, J. M. Pitarke, and J. B. Pendry, Phys. Rev. Lett. **78**, 4289 (1997).
[5] M. Kociak, L. Henrard, O. Stéphan, K. Suenaga, and C. Colliex, Phys. Rev. B **61**, 13 936 (2000); L. Henrard, O. Stéphan, M. Kociak, C. Colliex, and P. Lambin, J. Electron Spectrosc. Relat. Phenom. **114–116**, 219 (2001).
[6] M. Kociak, O. Stéphan, L. Henrard, V. Charbois, A. Rothschild, R. Tenne, and C. Colliex, Phys. Rev. Lett. **87**, 075501 (2001).
[7] F. J. Wicks and D. S. O'Hanley, in *Hydrous Phyllosilicates (Exclusive of Micas)*, edited by S. W. Bailey, Reviews in Mineralogy (Mineralogical Society of America, Washington, 1988), Vol. 19, pp. 91–167.
[8] C. Viti and M. Mellini, Eur. J. Mineral. **9**, 585 (1997).
[9] V. C. Farmer, *The Infrared Spectra of Minerals* (Mineralogical Society, London, 1974).
[10] S. Yariv and L. Heller-Kallai, Clays Clay Miner. **23**, 145 (1975).
[11] C. Lemaire, F. Guyot, and B. Reynard (unpublished).
[12] M. K. Titulaer, J. C. van Miltenburg, J. B. H. Jansen, and J. W. Geus, Clays Clay Miner. **41**, 496 (1993).
[13] E. Balan, A. M. Saitta, F. Mauri, C. Lemaire, and F. Guyot, Am. Mineral. **87**, 1286 (2002).
[14] S. Baroni, S. de Gironcoli, A. D. Corso, and P. Giannozzi, Rev. Mod. Phys. **73**, 515 (2001).
[15] E. Balan, A. M. Saitta, F. Mauri, and G. Calas, Am. Mineral. **86**, 1321 (2001). The IR absorption can be obtained as an integral over space of $W(\varphi, r, \omega)$.